Article

Developmental Cell

Patterned Anchorage to the Apical Extracellular Matrix Defines Tissue Shape in the Developing Appendages of *Drosophila*

Graphical Abstract

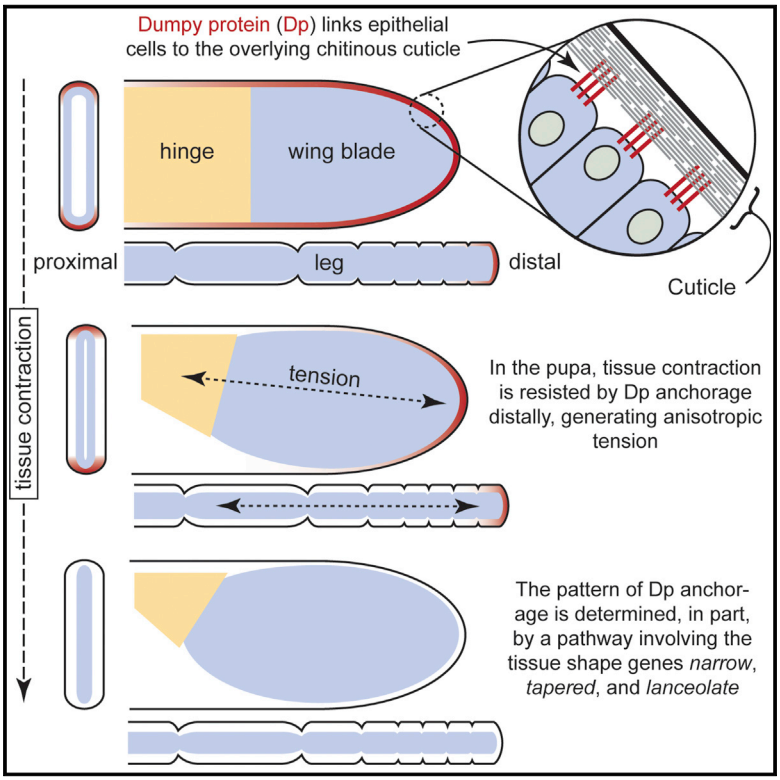

Highlights

- The apical extracellular matrix protein Dumpy (Dp) is required for appendage shape
- Dp anchors the epidermis to the cuticle, generating tension during tissue contraction
- Alteration of the pattern of Dp gives rise to predictable changes in appendage shape
- Narrow (Nw), Tapered (Ta), and Lanceolate (Ll) affect shape by modulating Dp

Authors

Robert P. Ray, Alexis Matamoro-Vidal, Paulo S. Ribeiro, ..., David Houle, Isaac Salazar-Ciudad, Barry J. Thompson

Correspondence

robert.ray@crick.ac.uk

In Brief

Regulation of global tensile forces in epithelia is one mechanism of determining tissue shape. Ray and Matamoro-Vidal et al. show that tissue contraction, in combination with localized anchorage to the cuticle by the apical extracellular matrix protein Dumpy, gives rise to anisotropic tensions that shape the appendages in the *Drosophila* pupa.

Ray et al., 2015, Developmental Cell *34*, 310–322
August 10, 2015
http://dx.doi.org/10.1016/j.devcel.2015.06.019

CellPress

CellPress

Developmental Cell
Article

Patterned Anchorage to the Apical Extracellular Matrix Defines Tissue Shape in the Developing Appendages of *Drosophila*

Robert P. Ray,[1,2,7,*] Alexis Matamoro-Vidal,[4,5,7] Paulo S. Ribeiro,[2,3] Nic Tapon,[2] David Houle,[4] Isaac Salazar-Ciudad,[5,6,8] and Barry J. Thompson[2,8]

[1]School of Life Sciences, University of Sussex, Falmer, Brighton BN1 9QG, UK
[2]The Francis Crick Institute, Lincoln's Inn Fields Laboratory, 44 Lincoln's Inn Fields, London WC2A 3PX, UK
[3]Centre for Tumour Biology, Barts Cancer Institute, Queen Mary University of London, Charterhouse Square, London EC1M 6BQ, UK
[4]Department of Biological Science, Florida State University, Tallahassee, FL 32306, USA
[5]Department de Genètica i Microbiologia, Genomics, Bioinformatics, and Evolution Group, Universitat Autònoma de Barcelona, Cerdanyola del Vallès 08193, Spain
[6]Center of Excellence in Experimental and Computational Developmental Biology, Developmental Biology Program, Institute of Biotechnology, University of Helsinki, P.O. Box 56, FIN-00014 Helsinki, Finland
[7]Co-first author
[8]Co-senior author
*Correspondence: robert.ray@crick.ac.uk
http://dx.doi.org/10.1016/j.devcel.2015.06.019

SUMMARY

How tissues acquire their characteristic shape is a fundamental unresolved question in biology. While genes have been characterized that control local mechanical forces to elongate epithelial tissues, genes controlling global forces in epithelia have yet to be identified. Here, we describe a genetic pathway that shapes appendages in *Drosophila* by defining the pattern of global tensile forces in the tissue. In the appendages, shape arises from tension generated by cell constriction and localized anchorage of the epithelium to the cuticle via the apical extracellular-matrix protein Dumpy (Dp). Altering Dp expression in the developing wing results in predictable changes in wing shape that can be simulated by a computational model that incorporates only tissue contraction and localized anchorage. Three other wing shape genes, *narrow*, *tapered*, and *lanceolate*, encode components of a pathway that modulates Dp distribution in the wing to refine the global force pattern and thus wing shape.

INTRODUCTION

Tissue morphogenesis depends on the precise control of basic cell behaviors such as cell division, cell death, cell shape, and cell rearrangement during development (Lecuit and Le Goff, 2007). While the regulation of cell proliferation and cell death in determining tissue size have been extensively studied (Edgar, 2006; Halder and Johnson, 2011), the mechanisms underlying the control of tissue shape are only just coming to light (Lecuit and Le Goff, 2007; St Johnston and Sanson, 2011; Zallen, 2007). In recent years, evidence has emerged for two types of mechanisms that influence tissue shape: active shape changes arising from intrinsic forces acting locally, which are integrated over the entire tissue to generate complex morphogenetic movements, and passive shape changes, which are driven by extrinsic forces that act globally to influence the behaviors of individual cells (Blanchard and Adams, 2011).

Morphogenetic processes driven by locally acting forces have been characterized in both plants and animals, and typically involve directed cell rearrangements, oriented cell divisions, or a combination of both (Lecuit and Le Goff, 2007). In vertebrate embryos, elongation of the anterior-posterior axis is driven in part by the polarized migration of mesenchymal cells that undergo convergent extension movements under control of planar cell polarity (PCP) genes (Heisenberg et al., 2000; Tada and Smith, 2000). A similar, PCP-dependent process has been implicated in the elongation of kidney tubules in *Xenopus* and mice (Lienkamp et al., 2012). In *Drosophila*, anterior-posterior (A/P) axis elongation also involves convergent extension movements that are driven by planar-polarized localization of Myosin II, which constricts epithelial junctions oriented along the dorsal-ventral axis. The resulting structures are then resolved into new A-P oriented junctions that drive extension of the germ band (Bertet et al., 2004; Blankenship et al., 2006; Irvine and Wieschaus, 1994; Zallen and Wieschaus, 2004).

Local forces can also affect tissue shape by influencing the orientation of cell divisions. This mechanism is best characterized in the *Drosophila* appendages, where elongation of the proximal-distal (P-D) axis is achieved by orientated cell divisions in the imaginal discs (Baena-López et al., 2005). P-D elongation in the discs results from the planar-polarized localization of the atypical Myosin, Dachs, by the Fat-Dachsous planar polarity system. Dachs constricts cell junctions where it is enriched, altering cell shape, and thus biasing the orientation of the mitotic spindle (Mao et al., 2011). Polarized cell divisions have also been implicated in other developmental processes including germ band extension in *Drosophila* (da Silva and Vincent, 2007), shoot

apex and petal morphogenesis in plants (Reddy et al., 2004; Roll-and-Lagan et al., 2003), and neurulation in zebrafish (Concha and Adams, 1998), but the molecular mechanisms underlying these examples remain to be determined.

There is also evidence for extrinsic forces acting across tissues to drive morphogenesis. In *Drosophila*, A-P tensile forces arising from convergence and extension of the underlying mesoderm have been implicated in driving cell shape changes in the ectoderm that contribute significantly to the fast phase of germ band extension (Butler et al., 2009). Similarly, in *Xenopus*, convergence and extension of deep mesenchymal cells generate forces that pull on the overlying epithelial cells, which, as a consequence, undergo passive intercalation (Keller, 2002). In zebrafish, actomyosin contraction within the yolk syncytial layer generates anisotropic tension in the enveloping cell layer that drives cell shape changes, cell rearrangements, and the orientation of cell divisions (Behrndt et al., 2012; Campinho et al., 2013). These findings highlight the potential importance of global tensile forces in animal morphogenesis, yet how these forces are controlled genetically remains unknown.

Here, we examine the genetic control of global forces using the *Drosophila* pupal wing as a model. Previous studies have shown that P-D elongation of the wing arises from passive orientation of cell divisions and cell rearrangements driven by global anisotropic tension imposed by cell constriction in the proximal part of the wing (Aigouy et al., 2010). We show that a group of well-known *Drosophila* mutants that affect wing shape disrupt components in a genetic pathway that acts to determine the pattern of global tensile forces in the wing. Central to this pathway is the apical extracellular matrix protein Dumpy (Dp) that links the pupal wing epithelium to the overlying pupal cuticle. The pattern of Dp localization at the crucial time of hinge contraction determines the ultimate shape of the wing. Our findings reveal a general mechanism for the control of tissue shape determination that has important implications for understanding the evolution of shape determination in animal systems.

RESULTS

The *dumpy* Gene Is Required to Shape the *Drosophila* Appendages

We sought to identify genes involved in defining the pattern of tensile forces in the pupal wing. We reasoned that hinge contraction could only result in anisotropic tension if the wing epithelium is anchored distally to provide the mechanical resistance necessary to give rise to the tension. Mutants that disrupt this anchoring should have the normal pattern of veins and interveins, but show a retraction of the wing blade toward the hinge. Such a phenotype is associated with alleles of the *dumpy* (*dp*) locus. Classical genetic studies on *dp* mutants revealed three phenotypic states for the locus: an oblique truncation of the wing (“o”), pits on the thorax known as vortices (“v”), and homozygous lethality (“l”). While the null phenotype of the locus is lethality, dp^{o} alleles as homozygotes or in combination with other alleles produce a continuous spectrum of wing phenotypes ranging from a mild flattening of the distal tip of the wing (the “oblique” phenotype), to a collapse of the distal tip (the eponymous “dumpy” phenotype), and, in the most extreme case, to a complete retraction of the wing blade (the “truncate” phenotype) (Figures 1A–1D) (Carlson, 1959). RNAi silencing of *dp* throughout the wing blade recapitulates the truncate phenotype with 100% penetrance (Figure 1E) and the same phenotype is produced with the *Dll-Gal4* driver, which is expressed at high levels only at the margin (Figure 1F). *Dll-Gal4* is also expressed in legs and antennae, and depleting *dp* in these tissues results in retraction of the distal segments of both appendages (Figures 1G and 1H), indicating that *dp* plays a general role in determining appendage shape.

The Dp Protein Is Localized to the Apical Extracellular Matrix and Is Restricted to Distal Regions of the Pupal Appendages

dp encodes a gigantic transmembrane protein that forms part of the apical extracellular matrix (aECM) and whose primary function is to anchor ectodermal cells to the overlying cuticle (Bökel et al., 2005; Jaźwińska et al., 2003; Wilkin et al., 2000). To characterize the distribution of Dp protein during appendage development, we have used a protein trap insertion into an N-terminal intron of *dp* that introduces a yellow fluorescent protein (YFP) tag into the extracellular domain of the protein, but does not affect protein function (dp-YFP, see Experimental Procedures). In the larval imaginal discs, Dp is found in a dense meshwork that uniformly covers the apical surface of the epithelium (Figure 2A). In the pupal wing, however, Dp is restricted. At the onset of hinge contraction (18 hr After Puparium Formation, APF), apically localized Dp is only found at the wing margin and to a lesser extent along the trajectories of the L3 and L5 veins (Figures 2B and 2E), while in the pupal leg and antenna, Dp is found at the extreme distal tip of the appendage (Figures 2J and 2K). As tissue contraction proceeds, de novo expression of Dp accumulates throughout the tissue (Figures 2C and 2D) such that, at 30 hr APF, it appears as a diaphanous network of enmeshed fibers that is similar in appearance to the aECM found in vertebrates (Figures 2F–2I) (Jovine et al., 2002).

Dp Anchors the Wing Margin to the Pupal Cuticle to Define the Pattern of Global Forces

Our results suggest a mechanism whereby the localization of Dp at 18 hr APF defines the pattern of attachment to the pupal cuticle. In support of this view, we find that in wild-type, the wing margin is attached to the overlying pupal cuticle during the early phase of hinge contraction, as has been observed previously for wings cultured in vitro (Turner and Adler, 1995). By contrast, in *dp* mutants, the wing is not attached and appears to float freely within the pupal cuticle (Figures 3A and 3B, arrows). Furthermore, the wing shape of *dp* mutants diverges from wild-type only during pupal development, as reported by Waddington (1940). At 18 hr APF, the size and shape of *dp* mutant wings are not substantially different from wild-type (Figures 3C and 3D). However, over the course hinge contraction, the *dp* mutant wing blade pulls away from the cuticle, and the tissue contracts into a rounded cup-shape that prefigures the shape of the adult wing (Figures 3C and 3D, bottom; cf. Figures 1A and 1E).

To further test the notion that final wing shape arises from the combination of tissue contraction and patterned anchorage of the wing margin, we developed a vertex model of the pupal wing epithelium that incorporates contraction of the hinge region with patterned attachment of the margin to a fixed cuticle

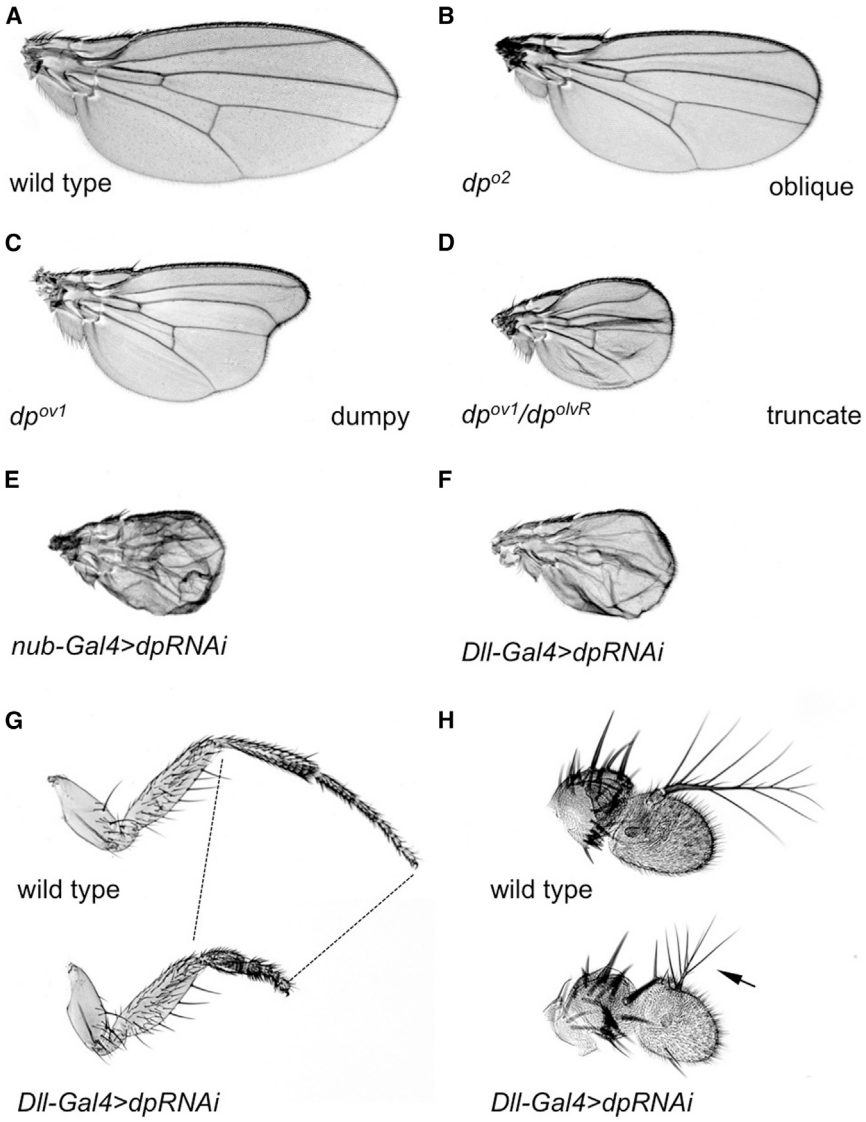

Figure 1. The *dp* Gene Is Required to Shape the *Drosophila* Wing, Leg, and Antenna

(A–F) Wing phenotypes associated with wild-type (A) or *dp* loss of function (B–F). The dp^{o} alleles produce wing phenotypes of differing severity: oblique (B), dumpy (C), and truncate (D). The silencing of *dp* by the expression of a UAS RNAi transgene in the entire wing blade with *nub-Gal4* (E) or along the wing margin with *Dll-Gal4* (F) recapitulates the truncate phenotype (E).

(G and H) The phenotypes associated with *Dll-Gal4>dpRNAi* in the second leg (G) and antenna (H) compared with the wild-type (top). As in the wing, *dp* knockdown results in a contraction of the distal part of the appendage.

substrate (Figures 3E and S5 and Movie S1). In the wild-type simulation, the hinge undergoes a contraction comparable to what is observed in vivo, and the blade responds by elongating along the P-D axis via oriented cell divisions and cell rearrangements, as described previously (Aigouy et al., 2010). If there is no attachment, the entire blade contracts, producing a wing shape that simulates the *nub-Gal4>dp-RNAi* phenotype (Figure 3F and Movie S1). These results indicate that the final shape of the wing can arise simply by the pattern of tensile forces resulting from tissue contraction and patterned anchorage.

Altering the Expression Pattern of Dp Predictably Affects Wing Shape

If the localization of Dp determines tissue shape during hinge contraction, then changing the pattern of Dp localization in the wing should result in predictable changes in shape. To test this, we silenced *dp* in defined patterns in the wing with the drivers *dpp-Gal4*, *sal-Gal4*, *brk-Gal4*, and *hh-Gal4*, thus generating novel patterns of *dp* anchorage (Figures 4A–4J). Knockdown of *dp* in the intervein between L3 and L4 with *dpp-Gal4* results in a retraction of the distal tip of the wing, where this intervein intersects with the margin (Figures 4B and 4G). A similar retraction of the distal tip of the wing is seen with *sal-Gal4>dp-RNAi*, but the phenotype is more severe, reflecting the broader expression of the driver (Figures 4C and 4H). Notably, this phenotype is similar to the dumpy phenotype associated with classical *dp* alleles (Figure 1C). RNAi depletion of *dp* in the complementary pattern with *brk-Gal4* results in a narrowing of the wing blade consistent with loss of anchorage along the anterior and posterior margins (Figures 4D and 4I), whereas silencing *dp* in the posterior compartment with *hh-Gal4* results in a contraction of the posterior part of the blade (Figures 4E and 4J). To address whether these phenotypes can arise as a result of alterations in the anchorage of the tissue, we incorporated the predicted patterns of Dp from each of our experiments into our computer model. The resulting simulated wing shapes resemble the corresponding in vivo phenotypes (Figures 4K–4O and Movie S2). These results indicate that the pattern of Dp attachment, coupled with contraction of the tissue, can account for the wing shape phenotypes observed in vivo.

Narrow, *Tapered*, and *Lanceolate* Affect Wing Shape

The tapered wing phenotypes we have observed with *brk-Gal4>dp-RNAi* and *hh-Gal4>dp-RNAi* are reminiscent of the wing phenotypes produced by three other loci, *narrow* (*nw*), *tapered* (*ta*), and *lanceolate* (*ll*), that were first identified early in the last century (Meyer and Edmondson, 1949; Morgan et al., 1925). Inactivation of these genes produces a range of phenotypes that can be generalized as a narrowing and lengthening of the wing. The phenotypes associated with *nw* alleles are dosage sensitive. Dominant antimorphic alleles (e.g., nw^{D}/+, nw^{B}/+) and weak hypomorphs produce a mild tapering of the distal part of the wing (Figures 5A and 5B), while recessive alleles

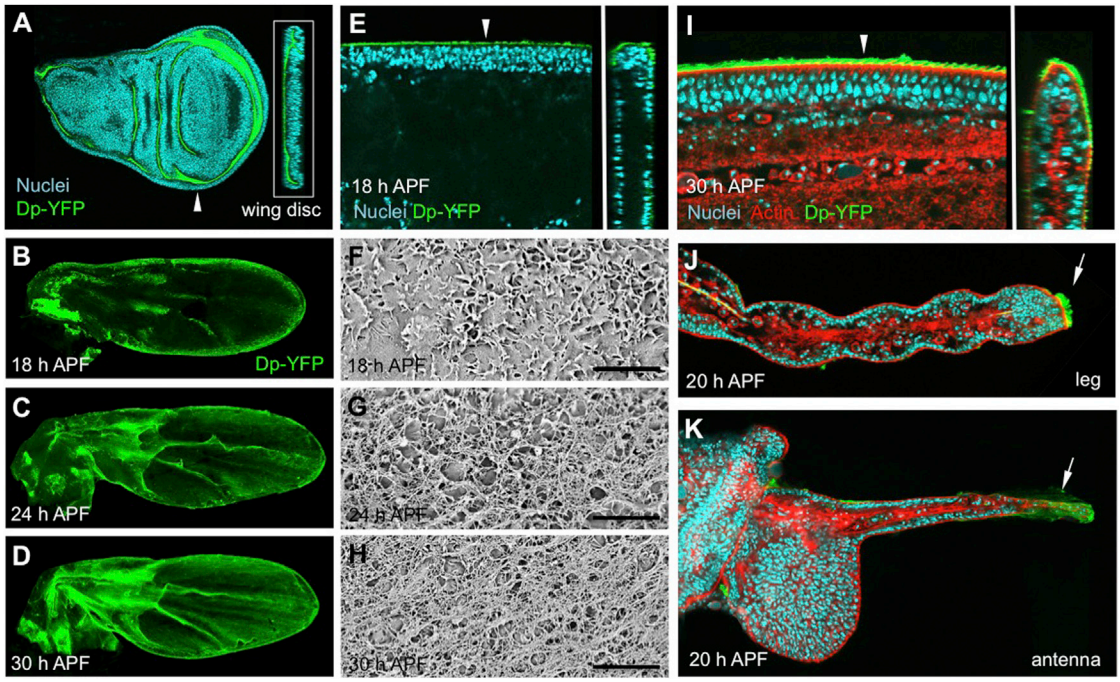

Figure 2. The Dp Protein Is an aECM Component that Is Specifically Localized during Morphogenesis

(A–G) Immunolocalization of Dp in the wild-type third instar wing disc (A), pupal wings during hinge contraction (B–E), in pupal legs (J), and antennae (K).

(A–G and J–K) Dp-YFP is shown in green, actin in red, and the nuclei in blue.

(A, E, and I) Insets show a z stack of the main image along the plane indicated by the arrowhead.

(A) In larval imaginal discs, Dp is expressed uniformly throughout the epithelium and is localized apically.

(B–E) In the pupal wing, expression is dynamic: at 18 hr APF, Dp is only found apically at the wing margin, with weak expression along the trajectories of L3 and L5 (B and E). Over the next 10 hr, Dp accumulates uniformly over the apical surface of the epithelium, so that by 30 hr APF, the protein appears in a diaphanous network overlying the actin-rich apical membrane (C, D, and I).

(F–H) SEM images reveal the development of the aECM network between 18–30 hr APF (the scale bar represents 5 microns). At 30 hr APF, the aECM is similar in appearance to the aECM that has been described in vertebrate systems. In the legs and antennae, Dp is also localized in the early stages of tissue contraction, with high levels of the protein detected at the extreme tip of the leg (J) and at the equivalent position in the antenna (K). (F)–(H) show SEM images of the pupal wing surface at the stages indicated.

give rise to the dramatic narrowing of the entire wing blade after which the gene is named (Figure 5C). The same range of phenotypes can be recapitulated by RNAi knockdown using *nub-Gal4* or *Tub-Gal4* (Figures 5D and 6A) to drive hairpin constructs directed toward different exons of the *nw* transcript (see Figure S2). Alleles of *ta* and *ll*, which are hypomorphic for the loci (see below), produce the weaker phenotype characteristic of the dominant alleles of *nw* (Figures 5E and 5F).

Morphometric analysis reveals that all of these phenotypes are associated with a simple shape warp that is, in essence, a stretch of the wing along the P-D axis. Depending on the genotypes included in the analysis, between 75%–85% of the variance is associated with a single principle component that constitutes an inward shift of landmarks along the anterior and posterior margins and an outward shift of landmarks at the distal tip of the wing (Figures S1A–S1D). Significantly, the change in blade shape is also associated with a contraction of the landmarks associated with the hinge. These data suggest that the stretch of the wing blade is associated with further contraction of the wing hinge than what is observed in wild-type. Notably, a corresponding deformation of the hinge is observed for any phenotype for which the pattern of Dp has been altered (see Figures 1A–1D and 4). Thus, for both *dp* and *nw* phenotypes, alterations in blade shape are associated with changes in hinge shape, suggesting that the cells of these two domains feed back on one another according to the pattern of tensile force on the tissue (see Discussion).

nw Encodes a Secreted C-type Lectin Domain Containing Protein

To investigate the function of these loci, we genetically and molecularly characterized the affected genes. Using standard deficiency mapping, *nw* was localized to a small region in cytological division 54A (Figure S2). RNAi of candidate genes in the interval identified a single gene, *CG43164*, that produced the *nw* phenotype when knocked down with the wing-specific driver *nub-Gal4* (Figure 5D). Confirming this result, two P-element insertions, G18887 and KG02048, that lie in the 5′ UTR of *CG43164* (Figure S2) fail to complement *nw* alleles, and sequencing of nw^{B}, nw^{D}, and nw^{DrS5} revealed lesions in the *CG43164* coding sequence, which we refer to hereafter as *nw* (Table S1, see also Figure S2).

The *nw* gene encodes a number of different mRNA species produced by differential initiation from a pair of nested promoters

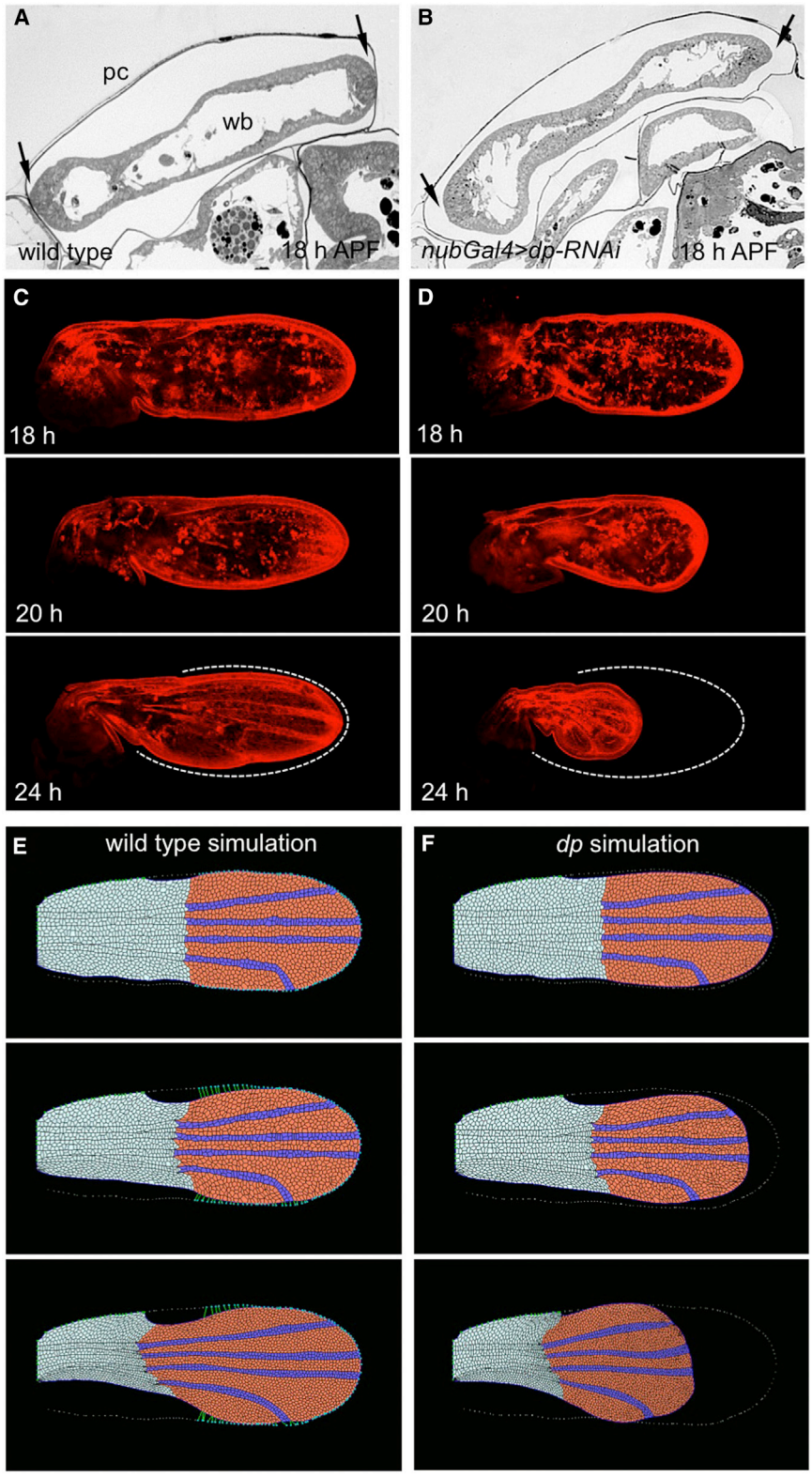

Figure 3. Dp Anchors the Wing Margin to the Pupal Cuticle to Define the Pattern of Global Forces that Shape the Wing

(A and B) Bright field images of frontal sections of wild-type (A) and *nub-Gal4>dp*-RNAi (B) wings at 18 hr APF, just after the pupal apolysis. In the wild-type, the anterior and posterior margin of the wing blade (wb), but not the dorsal and ventral surfaces, are attached to the overlying pupal cuticle (pc) (A, arrows), while in the *dp*-RNAi, the epithelium is fully detached (B, arrows). Consequently, phalloidin staining (red) reveals that the wild-type wing remains apposed to the cuticle during the period from 18–24 hr APF (C), while the *dp*-RNAi wing retracts proximally (D).

(C and D) The position of the cuticle is indicated in the final panel by a dashed white line.

(E and F) Epithelial vertex model of pupal wing morphogenesis. The starting point of the simulation is the early pupal wing shape, with the hinge region shown in light blue and the blade in red. The wing veins are shown in dark blue. The contraction of the tissue, most strongly in the hinge region, combined with anchorage of the wing margin (green lines) are sufficient to simulate wild-type wing morphogenesis. When the anchorage of the margin is absent in the computer model, the entire wing retracts, simulating the *dp* mutant wing (see Movie S1).

and by differential splicing and termination of the final exon. The various transcripts encode two protein isoforms, which we refer to as Nw-Short (Nw-S) and Nw-Long (Nw-L) (Figure S2). The two isoforms share a common N-terminal motif with homology to the C-Type Lectin Domain (CTLD). The core CTLD consists of four Cysteine (Cys) residues that are laid out with respect to a characteristic arrangement of α helices and β sheets. These Cys residues form intramolecular disulfide bridges that give rise to the double-loop fold characteristic of the domain (Zelensky and Gready, 2003) (Figure 5G). Additional Cys residues may also be present and, generally, if the number is even, all form intramolecular bonds, while if the number is odd, one of the Cys will form an intermolecular bond either with another CTLD protein or an unrelated protein (Drickamer and Dodd, 1999). The Nw CTLD contains five Cys residues, implying that one will form an intermolecular disulfide bridge, and given the placement of these residues with respect to the secondary structure, the final Cys is most likely to be involved in this bond (see Figure 5G).

We find that Nw-S and Nw-L are soluble, secreted proteins and either isoform can be immunoprecipitated from the culture medium when the *nw* gene is expressed in *Drosophila* S2 cells (Figure 5H). Under non-reducing conditions, the proteins run predominantly as higher molecular weight complexes that are approximately twice the size of the respective monomers, suggesting that they can form dimers. Additionally, when Nw-S and Nw-L are

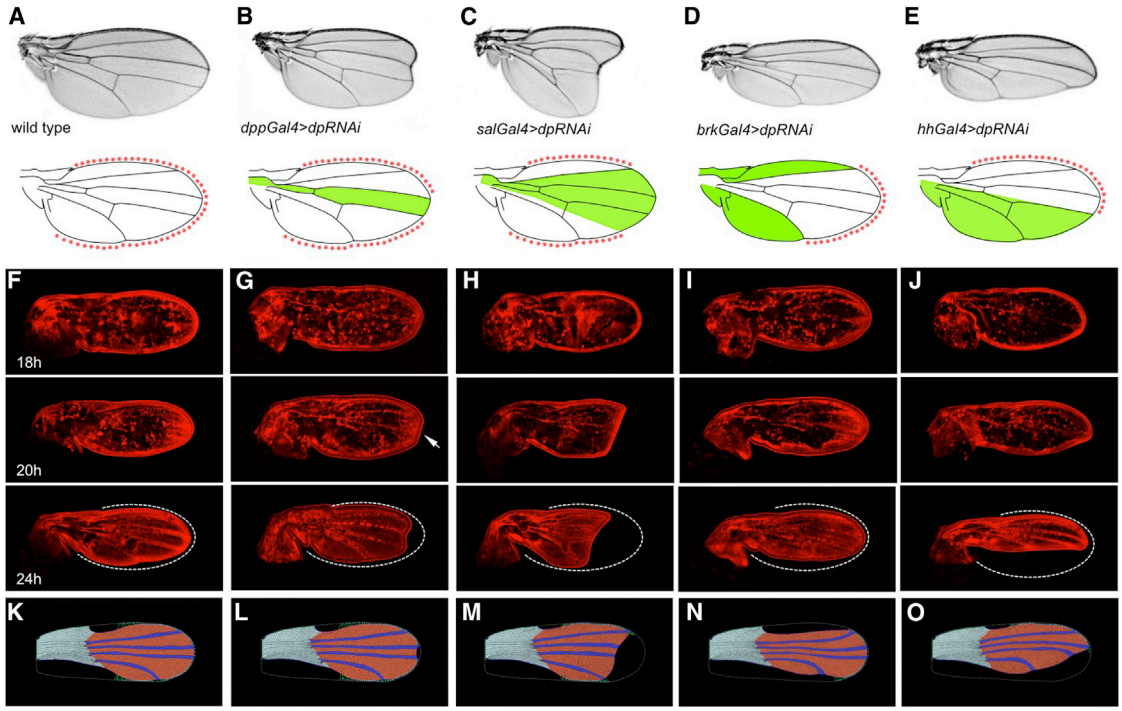

Figure 4. Altering the Pattern of Dp Gives Rise to Predictable Changes in Wing Shape

(A–E) Adult wing phenotypes for wild-type (A), localized silencing of Dp with *dpp-Gal4* (B), *sal-Gal4* (C), *brk-Gal4* (D), *hh-Gal4* (E) (top), diagrams showing the region of the wing where Dp is silenced (green), and the corresponding pattern of Dp anchorage (red asterisks) (bottom).

(F–J) Developmental time course of pupal wing development revealed by phalloidin staining (red) showing the ontogeny of the shape change from 18 to 24 hr APF. The position of the pupal cuticle with respect to the wing is shown in the final panel (dashed white line).

(K–O) The final images from the computational simulations of the genotypes corresponding to (A)–(E), using the epithelial vertex model (see Movie S2). The wing blade cells are shaded red, the hinge cells are shaded light blue, and the vein cells are shaded dark blue. The dashed white lines mark the wing outline at the beginning of the simulation. The Dp anchorage to the cuticle is shown as green lines ending with green dots and the anchorage in the hinge as green dots.

co-expressed, they form complexes corresponding to all possible homodimeric and heterodimeric combinations. The formation of these higher molecular weight complexes is dependent on the presence of the final Cys, as when this residue is mutated only the monomeric form is observed (Figure 5H). Finally, when FLAG-tagged Nw-S is co-expressed with HA-tagged Nw-S or Nw-L, immunoprecipitation with anti-FLAG antibodies co-precipitates the HA-tagged proteins (Figure 5H). Furthermore, if the final Cys is mutated (Cys > Ala), the modified protein is expressed, but cannot dimerize either with itself or the wild-type protein (Figure 5H).

ta and *ll* Are Required to Activate *nw*

Given the similarity between the mutant phenotypes of *nw*, *ta*, and *ll*, it was likely that the genes are part of a common biochemical pathway. Initial characterization of *ta* and *ll* by deficiency mapping, localized the loci to small intervals containing eight and nine genes, respectively (Figure S3). Considered separately, neither interval contained an obvious candidate for a protein that might interact with Nw. Considered together, however, two candidates were immediately apparent: the *ta* interval includes the *Drosophila* ortholog of Peptidyl-α-hydroxyglycine α-Amidating Lyase (*Pal1*), and the *ll* interval includes the ortholog of Peptidylglycine α-Hydroxylating Monooxygenase (*Phm*), the two components of the widely conserved Peptidylglycine α-Amidating Monooxygenase (PAM). Further characterization of the two loci confirmed this identification. The two *ll* alleles fail to complement Phm^{k07623} (Figure 5E), a P-element insertion into the *Phm* open reading frame, and they are associated with the same 10 bp deletion at the C terminus of the *Phm* protein that removes that final 26 amino acids (aa) and appends 79 aa or 80 aa from the second frame (Figure S3; Table S1). The ta^1 allele is associated with a nonsense mutation in the second coding exon of *Pal1* (Figure S3), and RNAi of *Pal1* in the developing wing phenocopies the *ta* mutant phenotype (Figure 5F; Table S1).

The α-amidation catalyzed by PAM is specific for a terminal glycine residue (Eipper et al., 1992), and consistent with Nw being a target for this modification, the short form of Nw (Nw-S) ends with a glycine residue that is universally conserved in all Nw orthologs. Furthermore, the modification is typically associated with small proteins, such as neuropeptides, whose function may be disrupted by the ionization of the terminal carboxyl group (Eipper et al., 1992). The fact that Nw-S is a small protein (194 aa), that is predicted to make a tight fold (Zelensky and Gready, 2005), makes it a likely target for α-amidation, and the mutant phenotypes of *ta* and *ll* indicate that this modification is essential for Nw function. Taken together, our data suggest that Nw, Ta, and Ll work in a common pathway, with the modifying enzymes being required for the maturation of Nw (Figure 5I).

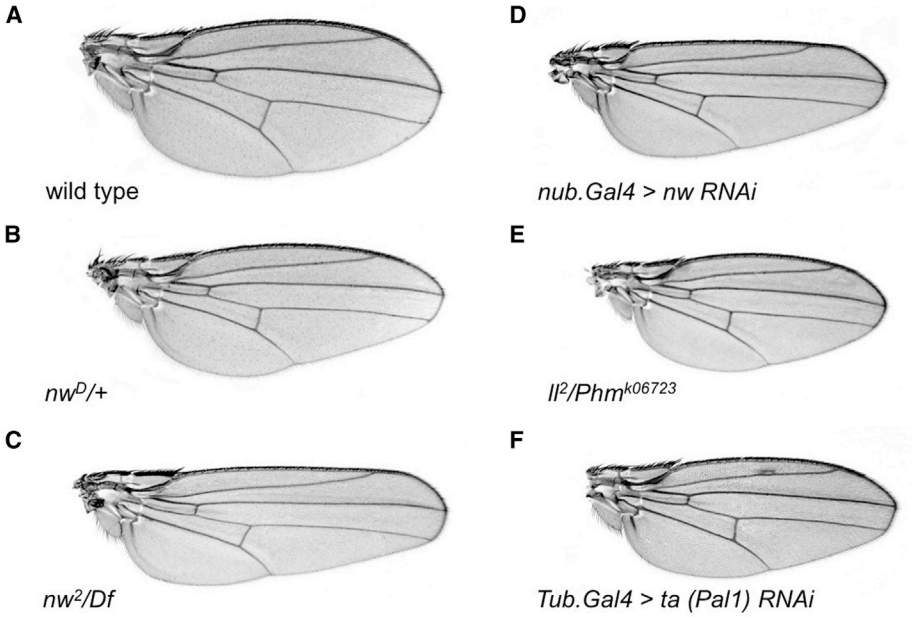

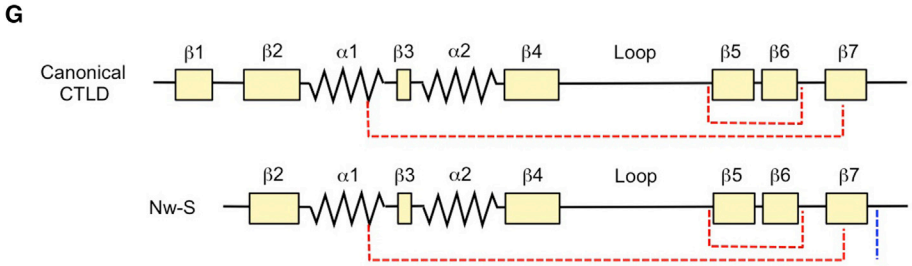

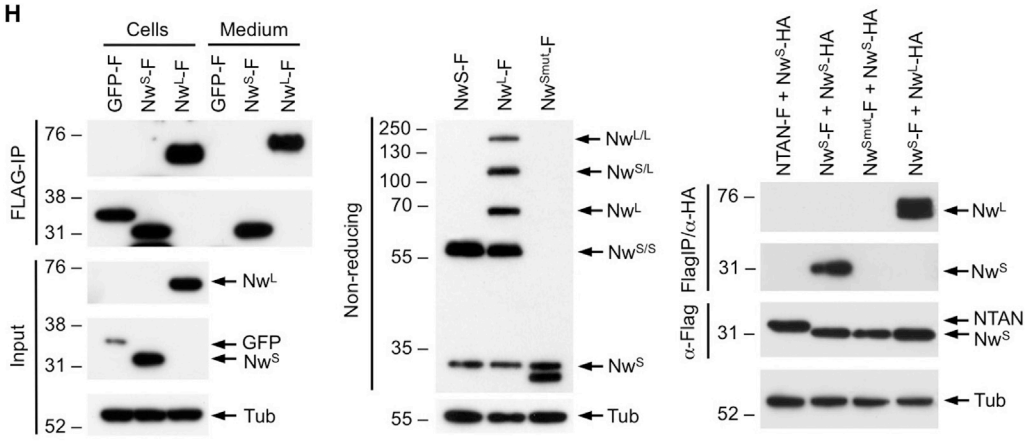

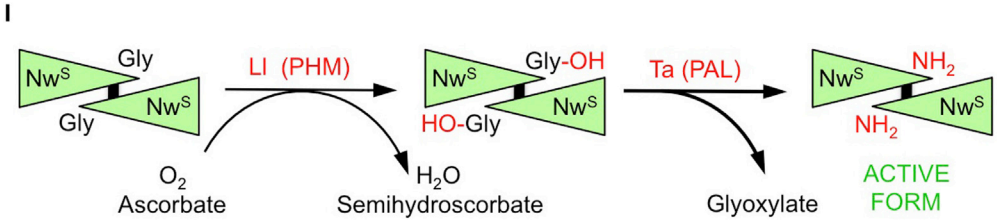

(legend on next page)

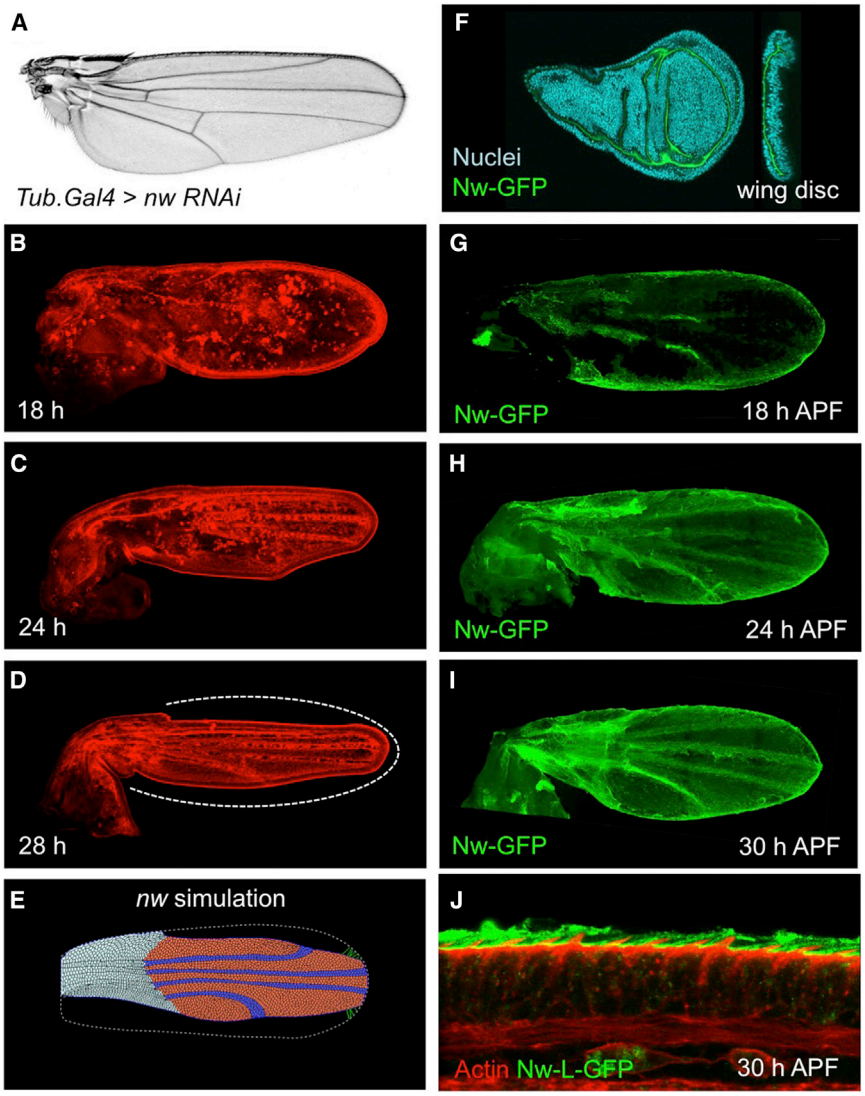

Figure 6. Localization of Nw in the Developing Wing and the Ontogeny of the Nw Phenotype

(A–E) Localization of Nw-GFP that has been expressed under control of the *nub-Gal4* driver. The Nw-GFP is shown in green, actin in red, and the nuclei in blue. Throughout wing development, Nw follows the pattern of Dp localization: in the wing disc, it is found apically throughout the epithelium, but at 18 hr APF, it is localized to the wing margin and the trajectories of L3 and L5 (B), as wing contraction proceeds, Nw accumulates uniformly throughout the wing blade in a diaphanous network overlying the actin-rich apical membrane and bristles (C–E; see also Figure S4).

(F–I) (F) Adult wing showing the phenotype associated with *Tub-Gal4>nw-RNAi* (A), which is similar to that produced by strong loss of function alleles of *nw* (see Figure 5C). Like the *dp* mutant phenotype (see Figure 3), the shape defect associated with *nw* mutants arises between 18–24 hr APF, concomitant with hinge contraction (G–I; cf. Figures 3C and 3D).

(J) Computational simulation of the *nw* mutant phenotype using the epithelial vertex model.

nw Affects the Localization of Dp to Control Wing Morphogenesis

The molecular characterization of *nw*, *ta*, and *ll*, and the mutant phenotype they produce, suggest that they might be involved in defining the localization of Dp in the developing wing. Consistent with this idea, the shape defect associated with *nw* mutants arises during hinge contraction (Figures 6A–6D), as we have observed for the *dp* mutations (cf. Figures 3C and 3D). In addition, the expression of a Nw-GFP fusion driven by the *nub-Gal4* driver precisely follows the pattern of Dp expression throughout wing development, despite the fact that fusion protein is expressed in all cells of the wing blade. In the wing disc, Nw is localized apically, in the pupal wing at 18 hr APF, it is localized to the wing margin and subsequently it accumulates uniformly in a fibrous network over the entire epithelium (Figures 6F–6J). Moreover, Nw-GFP does not localize to the aECM in *dp* mutant wings, in which the aECM fails to form properly (Figure S4). Finally, *nw* and *dp* interact genetically, with transheterozygotes producing wings that are either acutely tapered or retracted toward the hinge, similar to *dp* mutants (Figures 7A–7G). These results suggest that *nw* mutants affect wing shape by influencing the pattern of anchorage of the wing epithelium to the overlying cuticle.

Figure 5. The *nw*, *ta*, and *ll* Genes Control Wing Shape

(A–F) Adult wings showing shape phenotypes associated with *nw*, *ta*, and *ll* mutants. Compared to wild-type (A), the nw^D heterozygote (nw^D/+) is mildly tapered distally (B), while the recessive hemizygote (nw^2/*Df*) is narrower and longer (C), similar to what is observed with *nub-Gal4>nw-RNAi* (D). These phenotypes are associated with a single shape warp consisting of a stretch of the wing blade along the P-D axis (see Figure S1). The loss of function of *ll* (or Phm) or *ta* by RNAi knockdown results in a mild narrowing of the wing, similar to the phenotype produced by nw^D/+ (E and F).

(G) Molecular characterization of *nw* revealed that it encodes a CTLD protein (see also Figure S2), and secondary structure of the Nw-S protein compared to the canonical CTLD structure shows the two disulfide bridges (red dotted lines) that stabilize the characteristic fold of the motif, plus an additional Cys at the C terminus (blue dotted line), which is involved in dimerization.

(H) Biochemical analysis of Nw shows that both protein isoforms are secreted into the medium when expressed in tissue culture cells (left) and that under non-reducing conditions they are predominately found as homo- or hetero-dimers (right). Dimerization, but not synthesis or secretion, depends on the final Cys shown in (G): mutation of this Cys blocks both the formation of dimers and the ability of the mutant form to coIP the wild-type monomer (right).

(I) Molecular characterization of *ta* and *ll* (see Figure S3) reveals that they encode the two enzymes, Pal1 and Phm, that catalyze α-amidation, a post-translational modification that converts a C-terminal glycine residue into an α-amide. Nw-S terminates with a glycine and, given the phenotypes of *ta* and *ll*, α-amidation of this residue must be essential for Nw function in vivo.

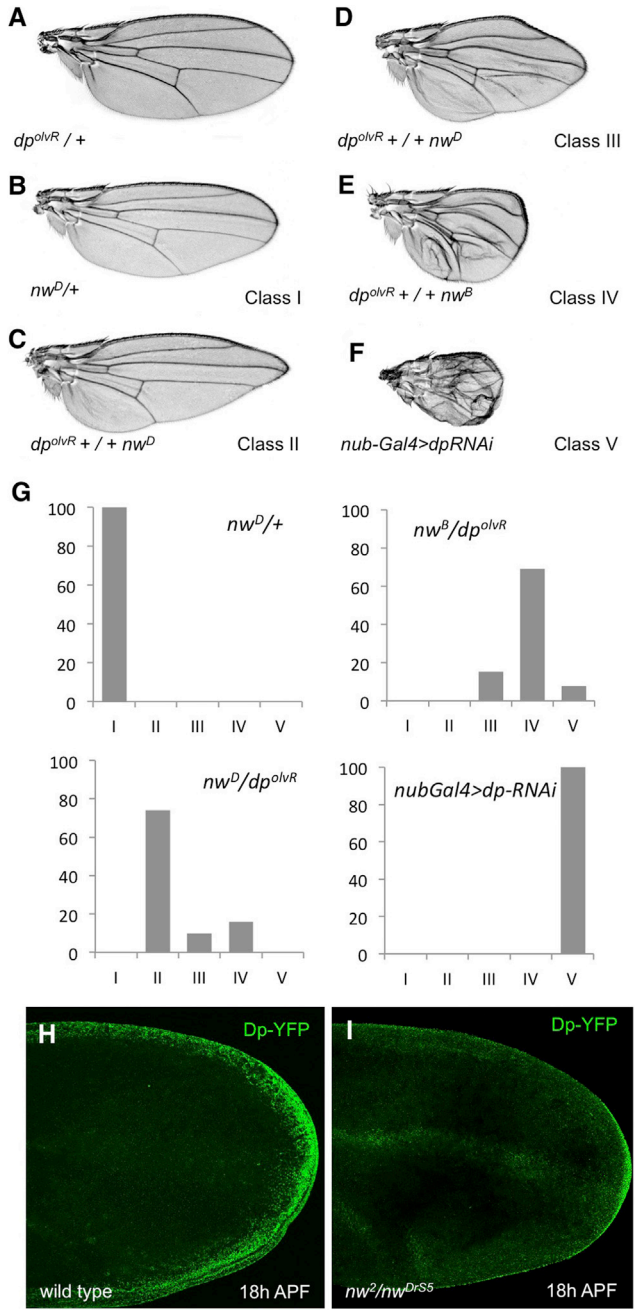

Figure 7. Genetic and Molecular Interactions between *nw* and *dp*

(A–F) The dosage sensitivity of *nw* makes it ideal for testing genetic interactions with other aECM proteins. *nw* shows a strong interaction with *dp*, but not with other aECM components (data not shown). A *dp* null heterozygote (dp^{olvR}/+) produces a wild-type wing (A), while the nw^D (or nw^B) heterozygote exhibits a mildly tapered wing (B). In the transheterozygous combination, dp^{olvR} +/+ nw^D, a spectrum of phenotypes is produced, ranging from sharply tapered to a complete retraction of the wing blade resembling the *dp* loss of function phenotype (C–F).

(G) Distinct phenotypic classes from this spectrum of phenotypes were defined to quantitate the enhancement, shown as percent of total wings showing the phenotype.

(H and I) Localization of Dp protein in wild-type (H) and *nw* mutant wings (I). In the wild-type, Dp protein is detectable throughout the wing margin, with higher levels at the distal tip (H). In the *nw* mutant wings, the expression is reduced to a small crescent of expression at the distal tip (I).

To investigate whether Nw has an effect on Dp, we examined the distribution of Dp-YFP in *nw* mutant wings. Given the *nw* phenotype, and the results from our simulations, we would predict that Dp is localized to the very distal tip of the wing. Indeed, in *nw* mutant wings at 18 hr APF, Dp-YFP is restricted to a narrow crescent at the extreme distal tip of the wing and is absent from the rest of the wing margin (Figures 7H and 7I). Moreover, the shape of the *nw* mutant wing can be simulated in our epithelial vertex model simply by restricting the anchorage of the wing margin to the distal tip (Figure 6E). Together, our data support a model where *nw* affects wing shape by altering the profile of the Dp localization at the onset of hinge contraction. The *nw, ta, ll*, and *dp* genes thus act together to define wing shape by controlling the pattern of global forces acting across the wing during pupal morphogenesis.

DISCUSSION

A Genetic Mechanism that Defines Tissue Shape

Here, we have identified a group of genes that define the global force patterns that shape the appendages in *Drosophila*. During pupal development, shape is determined by a general contraction of the tissue in combination with localized anchorage to the pupal cuticle, which is mediated by the aECM protein Dp. In the developing wing, Dp is localized to the wing margin such that, as tissue contraction proceeds, tension along the P-D axis elongates the wing and also draws the two wing surfaces together. Indeed, manipulating the pattern of Dp localization at this stage leads to dramatic changes in wing shape that reflect the underlying change in tissue anchorage. In the legs and antennae, Dp is found in a dense plaque at the distal tip of the appendage, and, as in the wing, tissue contraction results in tapering and elongation of the structure. Thus, we have identified a genetic mechanism that determines shape by regulating the pattern of global tensile forces that the epithelium experiences during tissue contraction.

Establishing the Pattern of Dp Localization

While the mechanism we have uncovered is clearly important for proper anchorage of the wing epithelium to the cuticle, it is only one part of the regulatory mechanism that leads to the localized attachment. Indeed, in a *nw* mutant, while the distribution of Dp is altered, it is still localized to the margin, thus other inputs must be involved in defining where Dp is localized during pupal development. In the wing, the localization of Dp to the margin is reminiscent of the expression of genes controlled by the Notch and Wingless pathways that define the dorsal-ventral compartment boundary. Indeed, the gene *Dll* is a downstream target of Wg, and knocking down *dp* in the cells that express *Dll* phenocopies the *dp* loss-of-function phenotype (Figure 1F). Moreover, the notching associated with mutations in the Notch and Wg pathways, as well as their targets such as *cut*, are, in essence, defects in the anchorage of the margin during pupal development: the failure to specify the margin results in a gap in the expression of Dp which produces a phenotype not unlike that which we observe in *dpp-Gal4>dpRNAi* (Figure 4B). Consistent with this, it has previously been shown that the notching associated with *cut* arises during pupal development during the period of hinge contraction (Jack et al., 1991). Thus, it may be that these

phenotypes arise from a failure to localize Dp to specific regions of the margin rather than to cell death, as has been suggested previously (Fristrom, 1968, 1969; Jack et al., 1991).

In the leg and antenna, the localization of Dp to the extreme distal tip of the appendage is presumably under control of the P-D patterning system that operates in these tissues. Indeed, as in the wing, we have shown that the retraction of the leg and antenna is produced by knocking down *dp* with *Dll-Gal4*, which is expressed in the most distal segments of both appendages (Campbell and Tomlinson, 1998). Moreover, the phenotypes we observe are also associated with mutations in genes that affect specification of the distal most tarsal segments. Classical loss-of-function mutations of the Paired-type homeodomain protein *aristaless* result in the same shortening of the arista as we observe with *dp-RNAi* (Campbell et al., 1993). Similarly, loss-of-function alleles of the transcription factor *Lim1* result in a shortening of the arista and the distal leg segments (Pueyo et al., 2000; Tsuji et al., 2000), which presumably reflects the failure to anchor the distal tip of the appendage to the pupal cuticle. Thus, we speculate that for wings, legs, and antennae, the localized function of Dp appears to depend on cues from the developmental programs that pattern the appendages.

While Dp localization clearly depends on the positional cues set down in the imaginal discs, how these signaling molecules and transcription factors result in a localized pattern of Dp protein in the pupa remains unclear. Previous studies have shown that the *dp* mRNA is expressed throughout the developing wing in early pupal development (Wilkin et al., 2000), suggesting that the localized pattern of Dp expression that is evident at 18 hr APF results by a post-transcriptional mechanism. Throughout development, Dp functions as a link between the ectodermal epithelium and the cuticle, and, in order for the animal to molt, this connection must be periodically broken. During larval development, molting (or *ecdysis*) is initiated by *apolysis*, a process that separates epidermal cells from the old cuticle by secretion of a complex mixture of chitinases and proteases that degrade the carbohydrate and protein components of the exoskeleton, respectively (Reynolds and Samuels, 1996). Given that Dp is essential for the link between epidermis and cuticle, it is a key target of the apolytic machinery. In the pupa, apolysis of the pupal cuticle occurs just prior to the onset of tissue contraction (Turner and Adler, 1995) and is a prerequisite for generating global forces by differential anchorage. Given this, the localization of Dp (Figure 2) and the localized anchorage of the appendage tissues to the cuticle (Figures 3A and 3B) presumably arise by protection of Dp at the margin and its degradation throughout the rest of the wing blade. Our results suggest that in the wing, Nw acts to extend this protection more proximally to give rise to the wild-type shape of the wing.

A Balance of Force, Resistance, and Fluidity in the Developing Appendages

Our results show that coordination of the behavior of thousands of individual cells in the pupal wing is achieved by the precise regulation of global extrinsic forces that determine appendage shape. In this system, the wing hinge undergoes apical constriction to generate a pulling force that is transmitted through the tissue. As we have shown here, resistance to this force is provided by anchorage of the wing margin to the overlying pupal cuticle, resulting in anisotropic tension oriented predominantly along the P-D axis. As has been shown previously, cells respond to this tension via cell shape changes, oriented cell divisions, and cell rearrangements to drive tissue elongation and determine the final shape the wing (Aigouy et al., 2010; Sugimura and Ishihara, 2013). Thus, as a mechanical process, tissue shaping during pupal development depends on the magnitude of the force generated by the constricting cells, the strength of the anchorage resisting this force, and the fluidity of the tissue to relieve the tension.

Several lines of evidence presented here suggest that these different components of the system operate toward an equilibrium state where opposing forces come to balance. For instance, if the force produced by the cell constriction exceeds the resistance, the anchorage ruptures, releasing the tissue. When this occurs, as in wings mutant for the hypomorphic allele dp^{ov1}, the margin collapses and the cells in the middle of the wing blade constrict further than they would otherwise (Figure 1C; Waddington, 1940). Similarly, the range of phenotypes observed in the interactions between nw^{D} and dp^{olvR} suggest that if the level of Dp falls below a certain threshold, the anchorage ruptures after hinge contraction has started, resulting in intermediate phenotypes that are flattened and retain some taper, but have nevertheless retracted (Figures 7D and 7E). These observations suggest that cells in the wing blade actively respond to the pattern of tensile force with significant consequences on wing shape.

Our data also indicate that hinge cells respond to the tension in the blade and constrict accordingly. Morphometric analysis of the *nw* mutant shows that the narrowing and extension of the wing blade is accompanied by a isometric contraction of the hinge, such that in the adult wing, the hinge is significantly smaller than in wild-type (Figures 5 and S1). Similarly, in the various *dp* mutants we have examined, any change in the wing shape is accompanied by a corresponding change in hinge size and shape (Figures 1, 4, and S1). The implication from these observations is that in the absence of sufficient resistance, hinge cells continue to undergo constriction, resulting in a corresponding change in hinge shape. Indeed, in our computational model, whenever the anchorage is released by any significant amount, the hinge is also found to contract further than in the wild-type simulation.

Taken together, these observations suggest that the system operates toward an equilibrium point where the force generated by hinge contraction is balanced with the resistance coming from the distal anchorage and the deformation properties of the cell matrix. Initially, the force generated by hinge contraction is offset by cell division and cell rearrangement, but when the cell division ceases, resistance in the epithelium feeds back on the hinge and eventually blocks further constriction. At this point, the system comes to equilibrium and the tension along the cell junctions equalizes. Notably, this model is consistent with previous reports, which have shown that after the initial phase of hinge contraction is completed, equalization of junction tension initiates the shift toward the hexagonal packing geometry that is characteristic of late stage pupal wings (Classen et al., 2005; Sugimura and Ishihara, 2013). The attractiveness of this kind of model is that it ensures robustness of the shaping mechanism and avoids the complications of tears or buckles that might arise from stochastic perturbations occurring during development. The nature of these feedbacks and how the equilibrium is achieved remain a question for further study.

The Nw-Dp System as a Target for Evolution of Shape

As orthologs of Dp and Nw have been found, and in all sequenced insect genomes and in the crustacean *Daphnia* (Carmon et al., 2007) (data not shown), our results suggest that the Nw-Dp system may be a key target for evolution of appendage shape in Arthropods. Indeed, given the tremendous variety of wing shapes that are found in insects, it is tempting to speculate that some of this variation is achieved by modulation of the Nw-Dp system, resulting in changes in the force patterns in the developing wing. For instance, in a recent report, wing shape differences in males of *Nasonia vitripennis* and *Nasonia giraulti* were attributed to differences in transcriptional regulation of an unpaired-like gene that was proposed to regulate proliferation in the developing wing (Loehlin and Werren, 2012). Significantly, the expression of this gene in both species was confined to the margin at the distal tip of the wing and strikingly prefigures the radius of curvature of the adult wing. Given our results, it is plausible that the difference in wing shape in these two species may arise from differences in anchorage of the wing tip, with the difference in cell number arising as a secondary consequence as in the case of *nw*. Similarly, the evolution of the diverse, specialized wing shapes in butterflies and moths has been attributed to defined expression of margin specific genes that prefigure the adult wing shape (Macdonald et al., 2010). While little is known of the elaboration of this prepattern during pupal development, the scalloping of the adult wing margin observed in many species—reminiscent of notching in the *Drosophila* wing—may well arise from precise deployment of the Nw-Dp system. Exploration of how Dp is regulated in different species may shed light on how the variety of insect wing shapes has evolved.

The aECM in Morphogenesis

In all metazoans, assembly of the aECM is dependent on proteins that contain a common protein motif, the Zona Pellucida (ZP) domain, which is thought to act as a polymerization module promoting the formation of homo and heterotypic filaments (Jovine et al., 2002). Genetic studies have implicated ZP-domain proteins in a variety of morphogenetic processes that typically involve shaping or remodeling of the apical domain of the cells (Plaza et al., 2010). In *Drosophila*, ZP-domain proteins shape the embryonic denticles and hairs (Fernandes et al., 2010) and the wing trichomes (Roch et al., 2003) that form on the apical surface of the cells, and in *C. elegans*, the Cuticlulins are ZP-domain proteins involved in the formation of the alae (Sapio et al., 2005). Similarly, in flies and nematodes, aECM proteins have been implicated as anchors in the cellular morphogenesis of sensory neurons, with *Drosophila* NompA functioning to anchor neural dendrites to the cuticular structures in sensory organs (Chung et al., 2001), while in the nematode, the aECM proteins DEX-1 and DYF-7 anchor the dendritic tips during cell body migration to shape the amphid sense organs (Heiman and Shaham, 2009). Among these examples, our findings represent a different paradigm for how aECM proteins can influence morphogenesis: rather than affecting the behavior of individual cells, and consequently the shape of the tissue, the Nw-Dp mechanism defines global force patterns across the tissue to which the individual cells respond to give rise to appendage shape.

In vertebrates, the most well studied ZP-domain proteins are the eponymous zona pellucida proteins that form the extracellular coat of mammalian ova (Jovine et al., 2002) and the α- and β-tectorins that are required for the formation of the tectorial membrane in the ear (Richardson et al., 2011). However, despite their importance for fertility and hearing, respectively, these proteins do not affect morphogenesis of the tissue per se. On the other hand, in the human kidney, the ZP-domain protein hensin/DMPT1 regulates morphogenesis of α- and β-Intercalated cells in the collecting tubules, and results from at least one study have found that global deletion of hensin results in embryonic lethality, suggesting a more general role in epithelial differentiation (Gao et al., 2010). Thus, there is mounting evidence from both invertebrates and vertebrates that the aECM plays an important role in morphogenesis and further studies on aECM proteins will undoubtedly reveal other roles they play in development and disease.

EXPERIMENTAL PROCEDURES

Drosophila Strains

The following stocks were used: nw^{2}, nw^{D}, nw^{B}, Df(2R)*BSC406*, ta^{1}, ll^{1}, ll^{2}, dp^{ov1}, and dp^{olvR} were obtained from the Bloomington Stock Center, and nw^{DrS5} was identified in a genetic screen for revertants of nw^{D}. *PBac{681.P.FSVS-1}*$dp^{CPTI001769}$ (*dp*-YFP) was obtained from the *Drosophila* Genetic Resource Center (Kyoto) and RNAi lines for *nw* (CG43164, line GD/49678), *dp* (GD/44029), and *Pal1* (KK103604) from the Vienna *Drosophila* Resource Center.

Wing and Cuticle Preparations

Wing, legs, and antennae were dissected from the body, washed in Isopropanol (Sigma), and mounted in DPX mounting medium (Fisher). Images were taken on a Zeiss Axioplan microscope fitted with a LeicaDFC420c digital camera.

Immunofluorescence, Microscopy, and Imaging

For larval wing discs, 120 hr larvae were cut in half and inverted in PBS and fixed in 4% formaldehyde (TAAB) in PBS for 20 min. After fixation, the inverted carcasses were permeabilized in PBS + 0.1% Triton X-100 and then blocked and stained as described below. For pupal wings, legs, and antennae, white prepupae were collected, aged, and then dissected from the pupal case, pierced with a forceps, and prefixed in 4% formaldehyde overnight at 4°C. After fixation, the pupal cuticle was removed and the relevant tissue dissected from the carcass.

For sections of whole pupae, appropriately aged pupae were pierced anteriorly with forceps and the posterior segments of the abdomen removed with dissection scissors. Using a micropipette, a solution of 4% paraformaldehyde was drawn through the carcass, removing much of the fat and internal organs, then transferred into 4% paraformaldehyde/2.5% glutaraldehyde in 0.1 M phosphate buffer (pH 7), and fixed for 1 hr before being post-fixed in 1% osmium tetroxide/1.5% potassium ferrocyanide overnight at 4°C. Samples were then treated with 1% tannic acid in 0.05 M sodium cacodylate for 45 min, washed in 1% sodium sulfate in 0.05 M sodium cacodylate for 5 min, and rinsed in water. Samples were dehydrated through a graded ethanol series and embedded in Epon 812 resin (TAAB). Semi-thin sections of 0.5 microns were cut using a UCT Ultramicrotome (Leica Microsystems), mounted on a glass slide and stained with toluidine blue. Images were taken on a Zeiss Axioplan microscope fitted with a LeicaDFC420c digital camera.

For scanning electron microscopy of pupal wings, pupae were dissected from the pupal case and fixed overnight in 4% paraformaldehyde/2.5% glutaraldehyde in 0.1 M phosphate buffer (pH 7) at 4°C. The pupal cuticle covering the wing was dissected away and the tissue was fixed for another 30 min at room temperature before washing 3 × 10 m in PBS. Samples were then dehydrated in 30%, 50%, 70%, 90%, and 100% ethanol (15 min each) followed by two washes in acetone prior to critical point drying. Samples were mounted on stubs, sputter coated, and viewed on a Phenom ProX scanning electron microscope.

For immunofluorescence, fixed tissues were blocked in PBS+0.1%Triton X-100+1% bovine serum albumin, incubated overnight at 4°C with primary antibody (anti-GFP, 1:300), and washed and incubated for 2 hr with secondary antibody (Alexa-488 anti-Rabbit 1:500). Tissue was then stained for 30 min with DAPI and Alexa-568-Phalloidin, washed, and then mounted in VECTASHIELD. Samples were imaged on a Leica SP5 confocal microscope.

Immunoprecipitation and Immunoblotting

For FLAG immunoprecipitation assays, cells were spun down and supernatant (cell culture medium) was collected. Where applicable, 10% of supernatant was processed for immunoblot analysis and the remainder used for FLAG immunoprecipitation as below. Cells were washed in cold PBS and lysed in lysis buffer (50 mM Tris [pH 7.5], 150 mM NaCl, 1% Triton X-100, 10% Glycerol, and 1 mM EDTA) supplemented with 0.1 M NaF, phosphatase inhibitor cocktails 1 and 2 (Sigma), and protease inhibitor cocktail (Roche). Cell extracts were spun at 14,000 rpm for 10 min at 4°C. FLAG-tagged proteins were purified using anti-FLAG M2 Affinity Agarose Gel (Sigma). After 1 hr incubation at 4°C, FLAG immunoprecipitates were washed 3–4 times with lysis buffer or wash buffer (10 mM Tris [pH 7.5], 150 mM NaCl, 0.1% Triton X-100, and 5% glycerol) and eluted using buffer supplemented with FLAG peptide. Sample Reducing Agent (Invitrogen) was omitted from samples prepared in non-reducing conditions. Detection of purified proteins and associated complexes was performed by immunoblot analysis using chemiluminescence (GE Healthcare). Western blots were probed with anti-FLAG (mouse M2, SIGMA), anti-HA (rat 3F10, Roche Applied Science), and anti-Tubulin (mouse E7, Developmental Studies Hybridoma Bank) antibodies.

Computational Model of Wing Development

To model the effects of global forces on whole wing morphology for the period from 18 hr APF to 28 hr APF, we extended the vertex model (Farhadifar et al., 2007; Honda et al., 2004) by incorporating hinge contraction and attachment of the margin to a fixed position (Figure S5; see Supplemental Information for a detailed description).

SUPPLEMENTAL INFORMATION

Supplemental Information includes Supplemental Experimental Procedures, five figures, one table, and three movies and can be found with this article online at http://dx.doi.org/10.1016/j.devcel.2015.06.019.

AUTHOR CONTRIBUTIONS

R.P.R. performed genetic, molecular, and immunohistochemical experiments, first in his own laboratory and, subsequently, as a visiting researcher in the laboratory of B.J.T. P.S.R. performed the biochemical studies on Nw. I.S.-C. and D.H. supervised the computational work, and I.S.-C. and A.M.-V. designed the computational model. A.M.-V. wrote the code and performed the analyses. R.P.R. and B.J.T. wrote the main body of the paper with contributions from the other authors. D.H., I.S.-C., and A.M.-V. co-wrote the Computational Methods section of the Supplemental Information.

ACKNOWLEDGMENTS

We thank Antonia Craig for preliminary work on the genetic characterization of *nw*; A. Weston for preparation and sectioning of whole pupae and scanning electron microscopy (SEM); and Y. Mao, M. Brun-Usan, J. Buceta, R. Farhadifar, M. Marin-Riera, and O. Shimmi for valuable help and discussions. This work was supported by a Wellcome Trust Investigator Award to B.J.T., a Genetics Society Summer Studentship and research grants from the BBSRC (BB/C508050/1) and MRC (G0500916) to R.P.R., an NIH grant (5R01GM094424-04) to D.H., and a Finnish Academy grant (WBS 1250271) to I.S.-C.

Received: October 24, 2014
Revised: April 2, 2015
Accepted: June 19, 2015
Published: July 16, 2015

REFERENCES

Aigouy, B., Farhadifar, R., Staple, D.B., Sagner, A., Röper, J.C., Jülicher, F., and Eaton, S. (2010). Cell flow reorients the axis of planar polarity in the wing epithelium of Drosophila. Cell *142*, 773–786.

Baena-López, L.A., Baonza, A., and García-Bellido, A. (2005). The orientation of cell divisions determines the shape of Drosophila organs. Curr. Biol. *15*, 1640–1644.

Behrndt, M., Salbreux, G., Campinho, P., Hauschild, R., Oswald, F., Roensch, J., Grill, S.W., and Heisenberg, C.P. (2012). Forces driving epithelial spreading in zebrafish gastrulation. Science *338*, 257–260.

Bertet, C., Sulak, L., and Lecuit, T. (2004). Myosin-dependent junction remodelling controls planar cell intercalation and axis elongation. Nature *429*, 667–671.

Blanchard, G.B., and Adams, R.J. (2011). Measuring the multi-scale integration of mechanical forces during morphogenesis. Curr. Opin. Genet. Dev. *21*, 653–663.

Blankenship, J.T., Backovic, S.T., Sanny, J.S., Weitz, O., and Zallen, J.A. (2006). Multicellular rosette formation links planar cell polarity to tissue morphogenesis. Dev. Cell *11*, 459–470.

Bökel, C., Prokop, A., and Brown, N.H. (2005). Papillote and Piopio: Drosophila ZP-domain proteins required for cell adhesion to the apical extracellular matrix and microtubule organization. J. Cell Sci. *118*, 633–642.

Butler, L.C., Blanchard, G.B., Kabla, A.J., Lawrence, N.J., Welchman, D.P., Mahadevan, L., Adams, R.J., and Sanson, B. (2009). Cell shape changes indicate a role for extrinsic tensile forces in Drosophila germ-band extension. Nat. Cell Biol. *11*, 859–864.

Campbell, G., and Tomlinson, A. (1998). The roles of the homeobox genes aristaless and Distal-less in patterning the legs and wings of Drosophila. Development *125*, 4483–4493.

Campbell, G., Weaver, T., and Tomlinson, A. (1993). Axis specification in the developing Drosophila appendage: the role of wingless, decapentaplegic, and the homeobox gene aristaless. Cell *74*, 1113–1123.

Campinho, P., Behrndt, M., Ranft, J., Risler, T., Minc, N., and Heisenberg, C.P. (2013). Tension-oriented cell divisions limit anisotropic tissue tension in epithelial spreading during zebrafish epiboly. Nat. Cell Biol. *15*, 1405–1414.

Carlson, E.A. (1959). Allelism, complementation, and pseudoallelism at the Dumpy locus in Drosophila melanogaster. Genetics *44*, 347–373.

Carmon, A., Wilkin, M., Hassan, J., Baron, M., and MacIntyre, R. (2007). Concerted evolution within the Drosophila dumpy gene. Genetics *176*, 309–325.

Chung, Y.D., Zhu, J., Han, Y., and Kernan, M.J. (2001). nompA encodes a PNS-specific, ZP domain protein required to connect mechanosensory dendrites to sensory structures. Neuron *29*, 415–428.

Classen, A.K., Anderson, K.I., Marois, E., and Eaton, S. (2005). Hexagonal packing of Drosophila wing epithelial cells by the planar cell polarity pathway. Dev. Cell *9*, 805–817.

Concha, M.L., and Adams, R.J. (1998). Oriented cell divisions and cellular morphogenesis in the zebrafish gastrula and neurula: a time-lapse analysis. Development *125*, 983–994.

da Silva, S.M., and Vincent, J.P. (2007). Oriented cell divisions in the extending germband of Drosophila. Development *134*, 3049–3054.

Drickamer, K., and Dodd, R.B. (1999). C-Type lectin-like domains in Caenorhabditis elegans: predictions from the complete genome sequence. Glycobiology *9*, 1357–1369.

Edgar, B.A. (2006). How flies get their size: genetics meets physiology. Nat. Rev. Genet. *7*, 907–916.

Eipper, B.A., Stoffers, D.A., and Mains, R.E. (1992). The biosynthesis of neuropeptides: peptide alpha-amidation. Annu. Rev. Neurosci. *15*, 57–85.

Farhadifar, R., Röper, J.C., Aigouy, B., Eaton, S., and Jülicher, F. (2007). The influence of cell mechanics, cell-cell interactions, and proliferation on epithelial packing. Curr. Biol. *17*, 2095–2104.

Fernandes, I., Chanut-Delalande, H., Ferrer, P., Latapie, Y., Waltzer, L., Affolter, M., Payre, F., and Plaza, S. (2010). Zona pellucida domain proteins remodel the apical compartment for localized cell shape changes. Dev. Cell *18*, 64–76.

Fristrom, D. (1968). Cellular degeneration in wing development of the mutant vestigial of Drosophila melanogaster. J. Cell Biol. *39*, 488–491.

Fristrom, D. (1969). Cellular degeneration in the production of some mutant phenotypes in Drosophila melanogaster. Mol. Gen. Genet. *103*, 363–379.

Gao, X., Eladari, D., Leviel, F., Tew, B.Y., Miró-Julià, C., Cheema, F.H., Miller, L., Nelson, R., Paunescu, T.G., McKee, M., et al. (2010). Deletion of hensin/DMBT1 blocks conversion of beta- to alpha-intercalated cells and induces distal renal tubular acidosis. Proc. Natl. Acad. Sci. USA *107*, 21872–21877.

Halder, G., and Johnson, R.L. (2011). Hippo signaling: growth control and beyond. Development *138*, 9–22.

Heiman, M.G., and Shaham, S. (2009). DEX-1 and DYF-7 establish sensory dendrite length by anchoring dendritic tips during cell migration. Cell *137*, 344–355.

Heisenberg, C.P., Tada, M., Rauch, G.J., Saúde, L., Concha, M.L., Geisler, R., Stemple, D.L., Smith, J.C., and Wilson, S.W. (2000). Silberblick/Wnt11 mediates convergent extension movements during zebrafish gastrulation. Nature *405*, 76–81.

Honda, H., Tanemura, M., and Nagai, T. (2004). A three-dimensional vertex dynamics cell model of space-filling polyhedra simulating cell behavior in a cell aggregate. J. Theor. Biol. *226*, 439–453.

Irvine, K.D., and Wieschaus, E. (1994). Cell intercalation during Drosophila germband extension and its regulation by pair-rule segmentation genes. Development *120*, 827–841.

Jack, J., Dorsett, D., Delotto, Y., and Liu, S. (1991). Expression of the cut locus in the Drosophila wing margin is required for cell type specification and is regulated by a distant enhancer. Development *113*, 735–747.

Jaźwińska, A., Ribeiro, C., and Affolter, M. (2003). Epithelial tube morphogenesis during Drosophila tracheal development requires Piopio, a luminal ZP protein. Nat. Cell Biol. *5*, 895–901.

Jovine, L., Qi, H., Williams, Z., Litscher, E., and Wassarman, P.M. (2002). The ZP domain is a conserved module for polymerization of extracellular proteins. Nat. Cell Biol. *4*, 457–461.

Keller, R. (2002). Shaping the vertebrate body plan by polarized embryonic cell movements. Science *298*, 1950–1954.

Lecuit, T., and Le Goff, L. (2007). Orchestrating size and shape during morphogenesis. Nature *450*, 189–192.

Lienkamp, S.S., Liu, K., Karner, C.M., Carroll, T.J., Ronneberger, O., Wallingford, J.B., and Walz, G. (2012). Vertebrate kidney tubules elongate using a planar cell polarity-dependent, rosette-based mechanism of convergent extension. Nat. Genet. *44*, 1382–1387.

Loehlin, D.W., and Werren, J.H. (2012). Evolution of shape by multiple regulatory changes to a growth gene. Science *335*, 943–947.

Macdonald, W.P., Martin, A., and Reed, R.D. (2010). Butterfly wings shaped by a molecular cookie cutter: evolutionary radiation of lepidopteran wing shapes associated with a derived Cut/wingless wing margin boundary system. Evol. Dev. *12*, 296–304.

Mao, Y., Tournier, A.L., Bates, P.A., Gale, J.E., Tapon, N., and Thompson, B.J. (2011). Planar polarization of the atypical myosin Dachs orients cell divisions in Drosophila. Genes Dev. *25*, 131–136.

Meyer, H.U., and Edmondson, M.E. (1949). New mutants report. D.I.S. *23*, 60–61.

Morgan, T.H., Bridges, C.B., and Sturtevant, A.H. (1925). The genetics of Drosophila melanogaster. In Bibliogr. Genet, *Second Volume*Bibliogr. Genet (Martinus Nijhoff Publishers), p. 262.

Plaza, S., Chanut-Delalande, H., Fernandes, I., Wassarman, P.M., and Payre, F. (2010). From A to Z: apical structures and zona pellucida-domain proteins. Trends Cell Biol. *20*, 524–532.

Pueyo, J.I., Galindo, M.I., Bishop, S.A., and Couso, J.P. (2000). Proximal-distal leg development in Drosophila requires the apterous gene and the Lim1 homologue dlim1. Development *127*, 5391–5402.

Reddy, G.V., Heisler, M.G., Ehrhardt, D.W., and Meyerowitz, E.M. (2004). Real-time lineage analysis reveals oriented cell divisions associated with morphogenesis at the shoot apex of Arabidopsis thaliana. Development *131*, 4225–4237.

Reynolds, S.E., and Samuels, R.I. (1996). Physiology and biochemistry of insect moulting fluid. Adv. Insect Physiol. *26*, 157–232.

Richardson, G.P., de Monvel, J.B., and Petit, C. (2011). How the genetics of deafness illuminates auditory physiology. Annu. Rev. Physiol. *73*, 311–334.

Roch, F., Alonso, C.R., and Akam, M. (2003). Drosophila miniature and dusky encode ZP proteins required for cytoskeletal reorganisation during wing morphogenesis. J. Cell Sci. *116*, 1199–1207.

Rolland-Lagan, A.G., Bangham, J.A., and Coen, E. (2003). Growth dynamics underlying petal shape and asymmetry. Nature *422*, 161–163.

Sapio, M.R., Hilliard, M.A., Cermola, M., Favre, R., and Bazzicalupo, P. (2005). The Zona Pellucida domain containing proteins, CUT-1, CUT-3 and CUT-5, play essential roles in the development of the larval alae in Caenorhabditis elegans. Dev. Biol. *282*, 231–245.

St Johnston, D., and Sanson, B. (2011). Epithelial polarity and morphogenesis. Curr. Opin. Cell Biol. *23*, 540–546.

Sugimura, K., and Ishihara, S. (2013). The mechanical anisotropy in a tissue promotes ordering in hexagonal cell packing. Development *140*, 4091–4101.

Tada, M., and Smith, J.C. (2000). Xwnt11 is a target of Xenopus Brachyury: regulation of gastrulation movements via Dishevelled, but not through the canonical Wnt pathway. Development *127*, 2227–2238.

Tsuji, T., Sato, A., Hiratani, I., Taira, M., Saigo, K., and Kojima, T. (2000). Requirements of Lim1, a Drosophila LIM-homeobox gene, for normal leg and antennal development. Development *127*, 4315–4323.

Turner, C.M., and Adler, P.N. (1995). Morphogenesis of Drosophila pupal wings in vitro. Mech. Dev. *52*, 247–255.

Waddington, C.H. (1940). The genetic control of wing development in Drosophila. J. Genet. *41*, 75–139.

Wilkin, M.B., Becker, M.N., Mulvey, D., Phan, I., Chao, A., Cooper, K., Chung, H.J., Campbell, I.D., Baron, M., and MacIntyre, R. (2000). Drosophila dumpy is a gigantic extracellular protein required to maintain tension at epidermal-cuticle attachment sites. Curr. Biol. *10*, 559–567.

Zallen, J.A. (2007). Planar polarity and tissue morphogenesis. Cell *129*, 1051–1063.

Zallen, J.A., and Wieschaus, E. (2004). Patterned gene expression directs bipolar planar polarity in Drosophila. Dev. Cell *6*, 343–355.

Zelensky, A.N., and Gready, J.E. (2003). Comparative analysis of structural properties of the C-type-lectin-like domain (CTLD). Proteins *52*, 466–477.

Zelensky, A.N., and Gready, J.E. (2005). The C-type lectin-like domain superfamily. FEBS J. *272*, 6179–6217.